Agricultural Water Management 224 (2019) 105698

Contents lists available at ScienceDirect

Agricultural Water Management

journal homepage: www.elsevier.com/locate/agwat

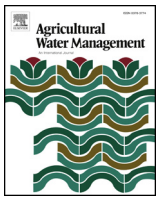

# Monitoring agricultural field trafficability using Sentinel-1

Coleen Carranza[a,*], Harm-jan Benninga[b], Rogier van der Velde[b], Martine van der Ploeg[a,c]

[a] Soil Physics and Land Management Group, Department of Environmental Sciences, Wageningen University, 6700 AA Wageningen, The Netherlands
[b] Water Resources Department, Faculty of Geo-Information Science and Earth Observation, University of Twente, 7500 AE Enschede, The Netherlands
[c] Hydrology and Quantitative Water Management Group, Department of Environmental Sciences, Wageningen University, 6700 AA Wageningen, The Netherlands

ARTICLE INFO

*Keywords:*
Agriculture
Soil moisture
Trafficability
Decoupling
Sentinel-1
Kernel density estimation

ABSTRACT

The use of heavy mobile machinery in agriculture for tillage and harvesting is now indispensable since it facilitates farming over large areas. However, one of the impacts of regular and prolonged use of heavy mobile machinery is soil compaction. To help minimize this harmful effect, trafficability of agricultural fields needs to be determined. Soil moisture acts as one of the dominant controls for field trafficability. Therefore satellites such as Sentinel-1, which is one source of spatio-temporal soil moisture information, could be useful in assessing trafficable conditions. One limitation of satellite-derived soil moisture is that only the upper surface layer is mapped. In this study, we determined the feasibility of Sentinel-1 surface soil moisture to monitor trafficability over 2016–2017. We first determined coupled conditions when surface soil moisture is a good indicator for values at the subsurface. We applied a probabilistic approach to determine trafficability using extensive in situ measurements of penetration resistance and surface soil moisture over a variety of crops. Trafficability is expressed as the probability that penetration resistance will exceed a threshold, for a given soil moisture value. Furthermore, we investigated the variability encountered from these measurements to gain insights on other temporal controls. Our results show coupled conditions for soil moisture $\geq 0.19\ cm^3\ cm^{-3}$ and there is an almost 1:1 correspondence between surface and subsurface values. For decoupled conditions, values at the subsurface can be two times more than the surface. An increase in penetration resistance variability coincided with the maturity of crops for cultivated fields. Aside from soil moisture, root growth may have a significant impact on the temporal variability of soil's penetration resistance. The status of trafficability can be monitored through the high temporal resolution of Sentinel-1. However, aggregation to coarser resolutions maybe necessary as its original 10 m resolution may be suboptimal, based on validation against in situ measurements. Days favorable for traffic were observed in early spring. This information can aid farmers in the timing of tillage activities or for water managers in deciding to adjust water levels to meet agricultural demands.

## 1. Introduction

Modern agriculture relies on heavy mobile machinery to carry out farming operations such as tillage and harvesting. Mechanization increases productivity and enables farming activities to be carried out over larger areas. This is driven both by the high demand for food production as well as economic factors to make agriculture profitable. However, one of the negative impacts of using heavy machinery is soil compaction (Lal, 1991; Raghavan et al., 1990; Hamza and Anderson, 2005; FAO, 2015). As a form of land degradation, soil compaction leads to structural damages to soil (Baumgartl and Horn, 1991; Eckelmann et al., 2006). Destruction of soil structure also leads to poor infiltration (Van Dijck and Van Asch, 2002) which in turn leads to water logging, run-off and erosion (Ekwue and Harrilal, 2010). Compaction can have negative consequences for crop root growth and soil ecosystems.

The use of heavy machinery in agriculture is indispensable so a balance in the timing of farming operations and susceptibility of soils to compaction must be achieved in order to minimize the harmful and long-term effects. A way to minimize the exposure to the negative impacts of using heavy machinery is to determine trafficable conditions for the soil. Assessment of agricultural field trafficability as well as the operating machinery during periods suitable for traffic can help slow down the rate at which soils are being compacted so that the use of heavy machinery can be sustainable in the long term. Trafficability is defined by Campbell and O'Sullivan (1991) as the ability of soil to (1) provide adequate traction for vehicles and (2) withstand traffic without excess compaction or structural damage. This is an extension to earlier studies for military purposes which were only concerned with vehicle

* Corresponding author.
*E-mail address:* coleen.carranza@wur.nl (C. Carranza).

https://doi.org/10.1016/j.agwat.2019.105698
Received 20 March 2019; Received in revised form 3 July 2019; Accepted 3 July 2019
Available online 21 August 2019

mobility (Knight and Freitag, 1961). More recent studies on field trafficability focus on soil–vehicle interaction to quantify the amount of soil compaction with different vehicle specifications (Keller and Lamandé, 2010; Nawaz et al., 2013; Rücknagel et al., 2015). Two sets of factors determine whether soils are able to support the weight of overlying machinery without increased risk for compaction. On the one hand are soil physical characteristics that dictate the mechanical strength of the soil. These include texture and bulk density of the soil (Müller et al., 2011). For soil texture, the strength of aggregated soils increases as clay content increases. Texture wise, soils with higher bulk density at the onset of field traffic can withstand higher pressures before undergoing deformation. Both soil texture and bulk density do not change significantly over short time scales (weeks or months) but they are important controls over the spatial patterns of trafficability. On the other hand are external factors that affect the grain-to-grain contact of individual soil particles. Perhaps the most important of these factors is soil moisture. For any given texture or bulk density, soil strength decreases towards wetter soil moisture conditions. Therefore soils become more prone to compaction with increasing soil moisture. The amount of overlying pressure that soils can accommodate decreases with increasing soil moisture since the grain-to-grain contact disappears as water fills up the pore space. Spatio-temporal soil moisture variability is influenced by atmospheric conditions (Seneviratne et al., 2010), soil properties (Rawls et al., 1991), and vegetation (Hupet and Vanclooster, 2002). Soil moisture exerts significant temporal control over soil strength as it varies greatly over short time scales because of changes in the prevailing atmospheric conditions. Other factors that control compaction are the set of vehicle specifications that determine the impacts of overlying machinery to the soil. Soil–vehicle interaction studies focus on the influence of tire inflation pressure, wheel and axle load on soil deformation (Müller et al., 2011).

The mechanical strength of the soil can be determined using cone penetrometers (Kuang et al., 2012; Upadhyaya, 2005). These are widely used instruments for determining soil's penetration resistance, which is equivalent to the force per unit base area required to push the cone penetrometer through a specified increment of soil depth (Bengough et al., 2000; ASAE EP542, 1999). They also have the advantage of providing relatively quick and easy measurements in the field. Cone penetrometer measurements are also referred to as cone index (CI). Existing field trafficability models have related soil moisture with CI using a decreasing exponential function (e.g. Henderson et al., 1988; Ayers and Perumpral, 1982; Sojka et al., 2001; Vaz et al., 2001), with an increasing CI trend towards drier soil moisture conditions. Several studies are geared towards monitoring and identifying conditions when the ground is less susceptible to compaction. For instance, Earl (1997) and Droogers et al. (1996) related trafficability and workability to soil hydraulic parameters to determine the number of workable days for a field. Other studies investigated the spatial variability of soil moisture and CI which can assist farmers in avoiding less trafficable areas within an agricultural field (Carrara et al., 2007; Ferrero et al., 2005). These studies have shown the impacts of soil moisture on field trafficability. Trafficability determined from soil moisture would be beneficial for agriculture, but this has been hampered in the past by the lack of continuous and available soil moisture data. Datasets from satellites are potential sources of regular and/or frequent soil moisture information that also cover a considerable spatial extent.

In the last few years, developments in mapping soil moisture using microwave remote sensing have been reported, with increasing spatial and temporal resolutions and accuracy (Kornelsen and Coulibaly, 2013; Vereecken et al., 2014). Techniques using microwave remote sensing are divided into active and passive methods. Passive microwave remote sensing measures the intensity of microwave emissions from the Earth's surface, expressed in terms of brightness temperatures. These measurements are performed with microwave radiometers. Active microwave remote sensing supply their own source of illumination. Active microwave sensors transmit signals towards a target and measures the portion scattered back. Synthetic aperture radar (SAR) is an active microwave sensing technique providing observations with a higher spatial resolution. SAR backscatter signals depend on the technical configuration of the sensor as well as the geometric and dielectric properties of objects on Earth. For soils, dielectric properties are highly influenced by its moisture content (Cihlar and Ulaby, 1974).

Sentinel-1 satellites, which carry a SAR instrument, are promising sources of soil moisture information that would be suitable for mapping and monitoring field trafficability at field scale. Its revisit time can be up to 2–4 days for certain areas in Europe (Torres et al., 2012), which makes it highly suitable for monitoring changes in soil moisture. The acquired images are also freely and operationally available. Sentinel-1 measurements are only sensitive to soil moisture in the upper surface layer (~5 cm). However, assessment of trafficability requires soil moisture values over the topsoil or critical layer (Droogers et al., 1996; Earl, 1997; Priddy and Willoughby, 2006; Reintam et al., 2016). Although values used in literature vary, this corresponds roughly to the upper 20–30 cm of the soil layer. This means that surface soil moisture from Sentinel-1 needs to be translated into subsurface values before it can be used in certain applications. The vertical variability of soil moisture may lead to decoupling between surface and subsurface values (Capehart and Carlson, 1997; Carranza et al., 2018) wherein conditions in the former no longer represents those at the latter. This complicates the estimation of depth-average soil moisture needed for assessment of trafficability. Identifying coupled soil moisture conditions would be beneficial as it facilitates the use of satellite-derived surface soil moisture to assess field trafficability.

In this study, our main objective is to assess whether Sentinel-1-derived surface soil moisture can be used to monitor field trafficability. For Sentinel-1, several aggregation schemes were tested to determine the optimal pixel size. The accuracy of these aggregation schemes were validated against reference in situ measurements from two monitoring networks (Raam and Twente networks). Given the measurement depth limitations of Sentinel-1, we first aim to identify conditions when surface soil moisture values are good indicators of those at subsurface. In addition, the variability encountered from extensive penetration resistance measurements was analyzed in order to gain further insights on its temporal controls. A probabilistic approach is applied to express trafficability based on surface soil moisture and to incorporate variabilities encountered from in situ measurements. We demonstrate the results over a small site within the Raam catchment as an example to show the potential of Sentinel-1 for monitoring agricultural field trafficability.

## 2. Study area and datasets

### 2.1. Raam and Twente soil moisture networks

We utilized several locations within the existing soil moisture monitoring network in Twente (Dente et al., 2011) and Raam catchment (Benninga et al., 2018) as our study sites. These two networks contain stations covering the eastern (Twente network) and southeastern (Raam network) parts of the Netherlands (Fig. 1). They were installed previously to serve as validation sites for satellite-derived data products. Each station contains sensors that continuously monitor soil moisture over the soil profile. Soil moisture and temperature sensors (ECH2O EC-TM or 5TM) were installed at discrete depths below the surface (5, 10, 20, 40, and 80 cm). Measurement loggers store values every 15 min. For this study, we utilized year-long measurements from 2016–2017. In both monitoring networks, stations were installed in agricultural areas, at the edge or corner of a field to allow continuous measurements. Installation in the middle of the field was not permitted because of tillage, harvesting or grazing of animals. From the Twente network, three out of the 20 stations were utilized; from the Raam network, six out of the 15 stations were utilized as study sites. These were chosen to capture the variability in the crops encountered at the

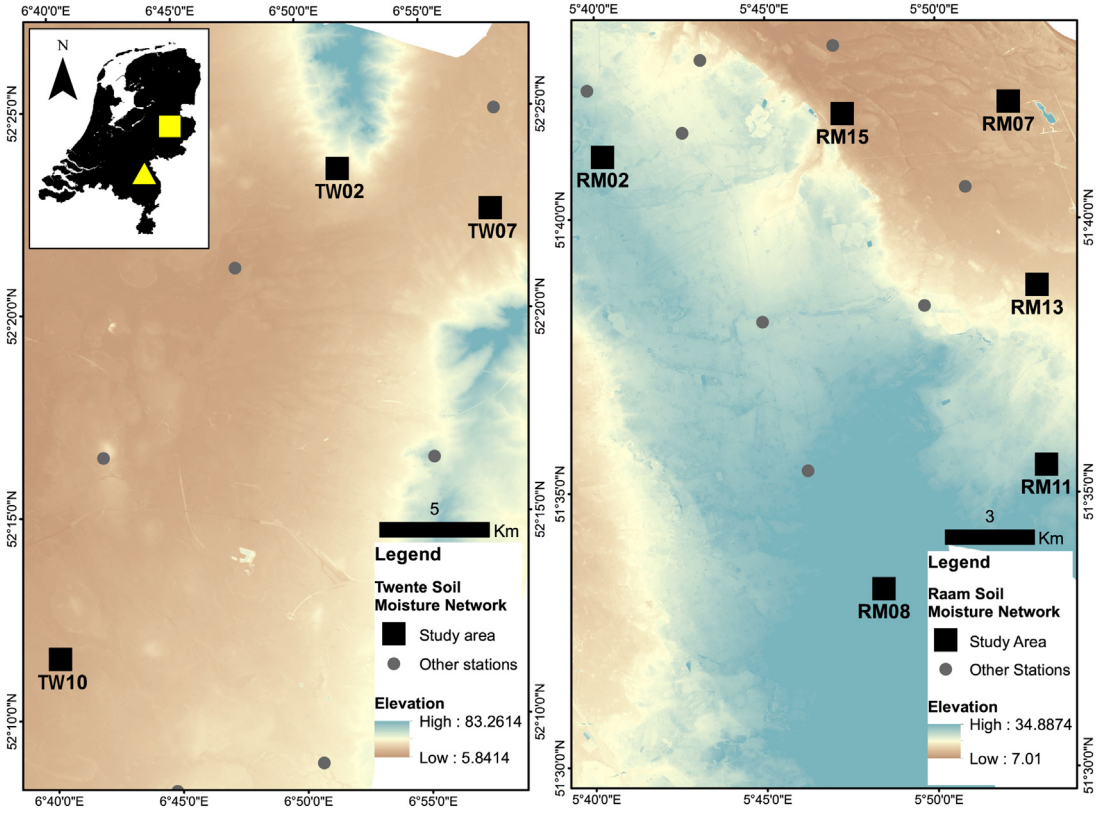


**Fig. 1.** Location of the study sites in Twente (yellow square) and the Raam (yellow triangle) soil moisture networks (inset). The stations utilized from Twente are plotted on the left while those from the Raam are plotted on the right. (For interpretation of the references to color in this figure legend, the reader is referred to the web version of this article.)

**Table 1**
Characteristics of the study sites. The description of soil types are taken from BOdemFysische EenhedenKaart (BOFEK 2012, (Wosten et al., 2013)). For the fields within Raam, the percentage of mineral components and organic matter content are taken from Benninga et al. (2018) while those from Twente are also from BOFEK 2012.

| Station No. | Soil description | %Silt | %Clay | %OM | Crop 2016 | Crop 2017 | Size (ha) |
|---|---|---|---|---|---|---|---|
| RM02 | Weakly loamy sandy soil on sub-soil of coarse sand (305) | 3.7 | 2.1 | 3.8 | Sugar beets | Winter Wheat | 2.96 |
| RM07 | Loamy sandy soil with thick man-made earth soil (317) | 10.5 | 5.2 | 2.2 | Corn/Cichory | Corn/Potato | 4.79 |
| RM08 | Weakly loamy podzol soil (304) | 1.6 | 1.4 | 4.1 | Sugar beets | Winter Wheat | 2.51 |
| RM11 | Weakly loamy podzol soil (304) | 1.7 | 1.6 | 1.9 | Corn | Corn | 3.49 |
| RM13 | Weakly loamy soil partly on sub-soil of coarse sand (309) | 1.1 | 0.8 | 1.4 | Corn | Grass | 8.48 |
| RM15 | Weakly loamy sandy soil with thick man-made earth soil (311) | 5.5 | 2.8 | 3.1 | Grass | Grass | 2.05 |
| TW02 | Loamy sandy soil with thick man-made earth soil (317) | 21 | 4 | 5.2 | Grass | Grass | 4.76 |
| TW07 | loamy sandy soil with a clay deck (316) | 35 | 13 | 2.4 | Winter Wheat | Corn | 4.55 |
| TW10 | Weakly loamy podzol soil (304) | 13 | 3 | 4.1 | Corn/Potato | Corn | 8.88 |

study sites during the two-year study period. The nine agricultural fields for this study were either grass or cultivated fields. The most common cultivated crop encountered was corn, followed by potato, sugar beet, winter wheat, and chicory (Table 1). The terrain in these fields was generally flat to gently sloping. Sandy soils were encountered in most of the fields, except for TW07 where the soil holds slightly higher loam content.

### 2.2. In situ surface soil moisture and cone index measurements

Aside from the soil moisture networks, we also collected in situ surface soil moisture and cone index measurements from the nine agricultural fields (Fig. 1). These were taken from two growing seasons, specifically from 26 May 2016 to 09 October 2017. For each growing season, a field was visited at least twice to collect measurements during different soil moisture conditions. The number of measurements ranged from 10 to 30 points per field per measurement day, depending on the size of the field. The points are 15–20 m apart and forms somewhat of a grid for each field. In addition, measurements were always taken at the same location for both surface soil moisture and penetration resistance. The measurement locations were also kept the same during succeeding measurement days for a growing season. This was not feasible for both years because the changes in crop planted made it difficult to keep the locations of existing points. In total, 840 actual measurement points were collected over all study sites.

Surface soil moisture was measured using a hand held time domain reflectrometry (TDR) device (TRIME-IMKO) with 5 cm pins. The calibration of TDR for sandy soils at the study sites was performed against volumetric soil moisture values from undisturbed samples collected during several occasions within the whole field campaign (Fig. 2). A total of 127 sample points were used for calibration using linear regression. The calibrated volumetric soil moisture (VWC) is given by the function:

$$VWC = 0.797x + 0.114 \quad (1)$$

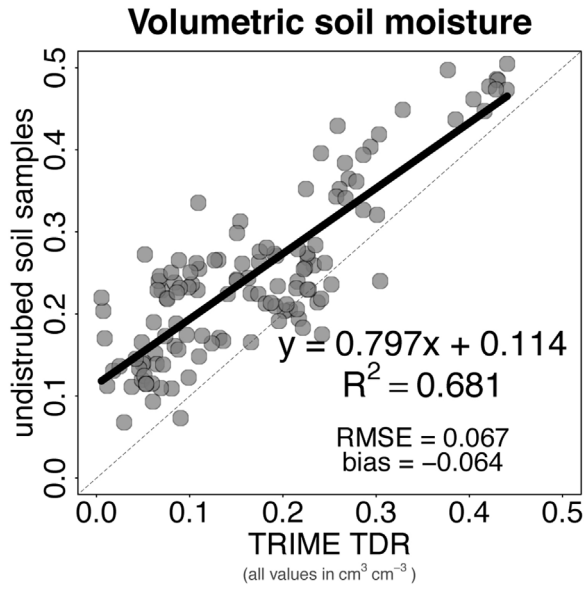


**Fig. 2.** Plot of volumetric soil moisture measured using TRIME TDR and undisturbed soil samples. Calibration of TRIME TDR measurements was performed by fitting a linear function of over the points. The fit is deemed reasonable based on an $R^2$ value of ~0.7. Values for bias and RMSE are also in $cm^3cm^{-3}$.

where $x$ is the soil moisture measured using the TDR device. The linear function used adequately fitted the points based on $R^2 = 0.681$. In addition, $RMSE = 0.067\ cm^3\ cm^{-3}$ indicated small differences between these two measurements and $bias = -0.064\ cm^3\ cm^{-3}$ indicated that measurements using the TDR device gave slightly lower readings compared to those from undisturbed samples.

Penetration resistance measurements were obtained using a hand held penetrometer (Eijkelkamp Penetrologger) with a 1 cm cone diameter and a 60 degree angle. We referred to the penetration resistance measurements also as the cone index (CI). The measurements were taken from the soil surface until 20 cm for every 1 cm-depth interval.

### 2.3. Sentinel-1 imagery

The SAR instrument on board the Sentinel-1 satellites operates in C-band (5.405 GHz), which in Interferometric Wide Swath (IW) mode provides over land images at VV and VH polarization, with pixel spacing of 10 m × 10 m and a reported radiometric accuracy of 1 dB ($3\sigma$) (Torres et al., 2012). Sentinel-1A and Sentinel-1B provide images since 3 October 2014 and 26 September 2016, respectively. The combination of Sentinel-1A and Sentinel-1B results in a revisit time of 3 days over the Raam study area and a revisit time of 1.5 days over the Twente study area. Given the higher sensitivity to soil moisture of backscatter observations acquired in VV polarization than in VH polarization (e.g. Baghdadi et al., 2017; Bousbih et al., 2017; Hajj et al., 2017), we used the observations in VV polarization to retrieve soil moisture. The Sentinel-1 images are freely available via the Copernicus Open Access Hub (ESA, 2019).

We applied the following operations to convert raw pixel values into radar backscatter ($\sigma$): (1) Range Doppler Terrain Correction (RDTC) using the tool in the Sentinel Application Platform (SNAP) software, which includes (a) radiometric calibration, (b) reprojection to correct for distortions due to topographical variations and tilt of the satellite sensor, and (c) radiometric normalization with projected local incidence angles, and (2) a 5 × 5 median speckle filter to suppress speckle noise.

Projected local incidence angles of the Sentinel-1 observations vary between 36.8° and 40.7° for the Raam study area and 31.5° and 46.7° for the Twente study area. We normalized the backscatter observations to a reference angle of 40° using a cosine correction (Ulaby et al., 1986):

$$\sigma^o_{\mathrm{ref}} = \sigma^o \frac{\cos^n(\varphi_{\mathrm{ref}})}{\cos^n(\varphi_{\mathrm{inc}})} \quad (2)$$

where $\sigma^o_{\mathrm{ref}}$ (in $m^2m^{-2}$) is the backscatter observation normalized to a reference angle $\varphi_{ref}$ of 40°, $\sigma^o$ is the backscatter observation (in $m^2m^{-2}$) and $\varphi_{inc}$ is the local projected incidence angle (in degrees). We assumed a value of $n = 2$, based on C-band SAR observations in previous studies (Lievens et al., 2011; Van der Velde and Su, 2009; Mladenova et al., 2013; van der Velde et al., 2015), which corresponds to the assumption that re-radiation from the soil surface follows Lambert's cosine law (Ulaby et al., 1986). Sentinel-1 observations that exceed the upper limit of −2 dB or the lower limit of −22 dB (the maximum noise equivalent sigma zero) were taken out.

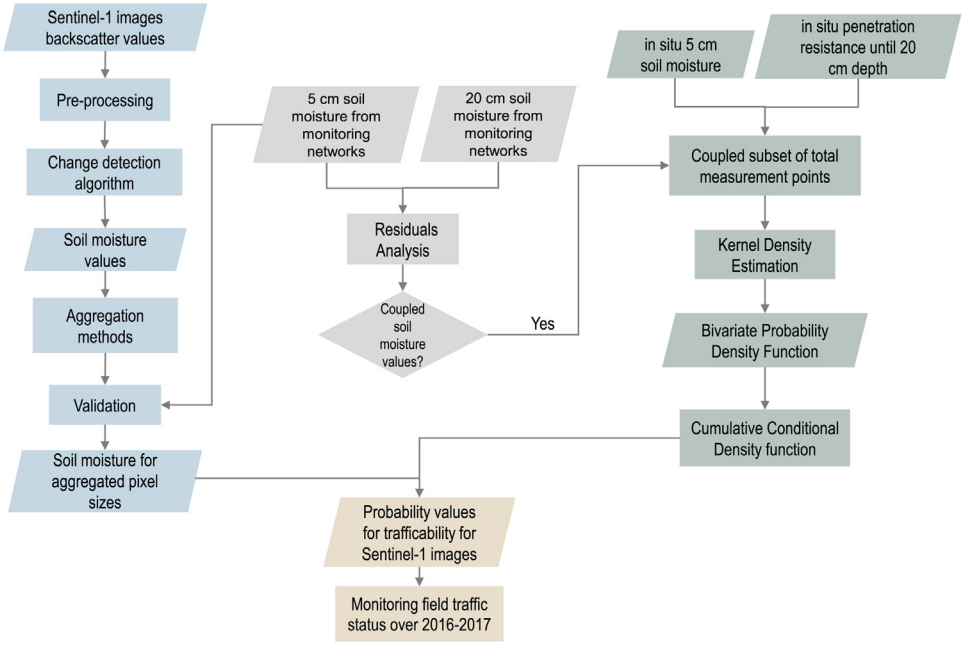


**Fig. 3.** Flowchart summarizing the methods applied in this study. The analysis was carried out in three parts. One section focuses on translating Sentinel-1 backscatter to soil moisture values and validating the results with in situ time series measurements. Another section focuses on determining coupled soil moisture conditions. The third section describes the probabilistic framework applied to express trafficability using surface soil moisture and penetration resistance values.

## 3. Methods

The analysis carried out for monitoring field trafficability using Sentinel-1 was divided into three parts (Fig. 3). The first section describes the soil moisture retrieval from Sentinel-1 backscatter values. This section also includes the validation of soil moisture retrievals using time series field measurements. The second section describes the coupling of surface and topsoil soil moisture values by looking at the variability between the two. This was needed in order to identify which surface soil moisture values (e.g. derived from Sentinel-1) are representative for the total soil moisture content within the topsoil. Using these results, the third section describes the probabilistic framework applied to express field trafficability using in situ measurements of surface soil moisture and cone index.

### 3.1. Soil moisture retrieval – change detection algorithm

The change detection algorithm, developed by Wagner et al. (1999), linearly relates backscatter (in dB) to a relative soil moisture index $S_w$ of the surface layer over time:

$$S_w(t) = \frac{\sigma^o_{40^o}(t) - \sigma^o_{40^o,\mathrm{Min}}}{\sigma^o_{40^o,\mathrm{Max}} - \sigma^o_{40^o,\mathrm{Min}}} \quad (3)$$

where $\sigma^o_{40^o,\mathrm{Min}}$ and $\sigma^o_{40^o,\mathrm{Max}}$ are the backscatter observations under dry and wet soil conditions (in $cm^3cm^{-3}$), respectively. The absolute minimum and maximum values of $\sigma^o_{40^o}$ are probably outliers due to radiometric noise, speckle or exceptional surface conditions, such as wet snow or surface inundation (Pathe et al., 2009; Bauer-Marschallinger et al., 2018). To exclude these outliers, we estimated the $\sigma^o_{40^o,\mathrm{Min}}$ and $\sigma^o_{40^o,\mathrm{Max}}$ by the 2.5% and 97.5% percentile of the time series. For the calculation of $\sigma^o_{40^o,\mathrm{Min}}$ and $\sigma^o_{40^o,\mathrm{Max}}$ we used time series of two complete hydrological years, between 1 March 2016 and 1 March 2018, resulting in 395 images over the Twente region and 198 over the Raam catchment. For backscatter observations that exceed $\sigma^o_{40^o,\mathrm{Min}}$ or $\sigma^o_{40^o,\mathrm{Max}}$, $S_w(t)$ is set equal to 0 or 1, respectively.

The main assumption of the change detection algorithm is that the parameters, other than soil moisture, are considered time-invariant, such as surface roughness and vegetation. The change detection algorithm is promising for operational applications of soil moisture retrievals from satellite observations, because the model is build only on a statistical analysis of backscatter time series and no detailed ground parameters are required (Wagner et al., 1999; Pathe et al., 2009; Hornacek et al., 2012; Bauer-Marschallinger et al., 2018). Although Wagner et al. (1999) developed the change detection algorithm for coarse satellite observations (European Remote Sensing scatterometer satellites, spatial resolution 50 km), several studies obtained acceptable correlations with in situ soil moisture measurements using SAR observations at C-band (Pathe et al., 2009; Hornacek et al., 2012; Bauer-Marschallinger et al., 2018).

The change detection algorithm results in a relative soil moisture estimate whereas absolute soil moisture, corresponding to the volumetric water content, is needed for mapping field trafficability. This problem is circumvented here by assuming that soil moisture varies between the wilting point ($\theta_{wp}$) and saturated soil moisture content ($\theta_{sat}$), which allowed us to linearly scale $S_w$ to volumetric soil moisture $\theta$ (in $cm^3cm^{-3}$), as follows:

$$\theta(t) = (\theta_{\mathrm{sat}} - \theta_{\mathrm{wp}})^* S_w(t) + \theta_{\mathrm{wp}} \quad (4)$$

The BOdemFysische EenhedenKaart (BOFEK2012) provides the soil type classes and associated soil physical characteristics (including van Genuchten parameters) for the soil units in the Netherlands (Wösten et al., 2001; Wosten et al., 2013). Then, the van Genuchten equation (van Genuchten, 1980) gives the soil moisture content at wilting point and saturated conditions (Table 2). Benninga et al. (2018) showed that the wilting point and saturated soil moisture content calculated from BOFEK2012 align with the minimum and maximum soil moisture measurements at 5 cm depth of the individual stations of the Raam network.

**Table 2**
Values of $\theta_{sat}$ and $\theta_{wp}$ derived from BOFEK 2012. These parameters were used to linearly scale relative $S_W$ values and derive absolute soil moisture values (see Eq. (4)).

| Station No. | BOFEK code | $\theta_{sat}$ | $\theta_{wp}$ |
|---|---|---|---|
| RM02 | 305 | 0.43 | 0.03 |
| RM07 | 317 | 0.45 | 0.05 |
| RM08 | 304 | 0.43 | 0.03 |
| RM11 | 304 | 0.43 | 0.03 |
| RM13 | 309 | 0.43 | 0.03 |
| RM15 | 311 | 0.43 | 0.03 |
| TW02 | 317 | 0.45 | 0.05 |
| TW07 | 316 | 0.40 | 0.12 |
| TW10 | 313 | 0.45 | 0.05 |

#### 3.1.1. Validation of Sentinel-1 estimates using in situ measurements

The accuracy of soil moisture retrievals were evaluated against reference soil moisture values at the study sites. We utilized the 5 cm soil moisture measurements from the nine stations as reference values to validate the soil moisture retrievals from Sentinel-1. A subset of the total dataset was obtained based on the common dates for both datasets. Aside from the original 10 m resolution, we tested four aggregation methods in order to determine the optimal pixel resolution for Sentinel-1. The first method employed aggregation to coarser resolutions of all the pixels in the Sentinel-1 image after masking out those which were not agricultural lands or low vegetation nature areas. For the second method, we aggregated only the pixels within each field boundary after masking out pixels outside each field. For the third method, we aggregated only the surrounding pixels, with the station located at the center. A circular buffer around each station was created to mask out the pixels outside the buffer. The fourth method involved calculation of the field mean. We aggregated the pixels to 50 m, 100 m, and 150 m, for each of the first three aggregation methods. The choice of upper limit (150 m) for aggregation was based on the size of the smallest field encountered at the study sites (Table 1) so that it is comparable to area of the largest pixel size used. The smallest field is at RM15 with an area of 2.05 ha while a 150 × 150 m pixel size has an area of 2.25 ha.

To select the optimal resolution and aggregation method for Sentinel-1, we calculated several performance metrics to compare the results. We computed RMSE, bias, unbiased RMSE, and Spearman's rank correlation coefficient for the results of aggregation methods used. The optimal resolution and aggregation method was further utilized to derive the trafficability status at selected fields over 2016–2017.

### 3.2. Soil moisture and cone index variability

#### 3.2.1. Vertical soil moisture variability

As the first step to relate satellite-derived surface soil moisture to field trafficability, we investigated when surface soil moisture is a good indicator of subsurface soil moisture conditions. We utilized the time series measurements at 5 cm and 20 cm from the selected study sites within Twente and Raam monitoring networks. The 5 cm values represent surface soil moisture measurements as they approximate the depths at which most satellites are able to extract soil moisture information. The 20 cm values correspond to measurements at the topsoil depth which carries the weight of overlying machinery. Several studies have also referred to such depths as the critical layer (Knight and Freitag, 1961; Paul and de Vries, 1979; Priddy and Willoughby, 2006). We referred to vertical variability as the irregularity between soil moisture values between 5 cm and 20 cm depths.

Using the time series soil moisture datasets from the Raam and

Twente monitoring networks, we applied residuals analysis to look at (de)-coupling between surface and topsoil moisture conditions. Carranza et al. (2018) inferred that there is lower vertical variability during coupled soil moisture conditions. The analysis involved fitting a non-parametric loess function to relate surface and topsoil values. After which, residuals from the fitted loess function were used to calculate the residuals variance. This showed the vertical variability throughout the whole soil moisture range encountered at the study sites. To determine whether coupling or decoupling is present given any soil moisture value, the cumulative residuals variance line was plotted. This allowed us to observe changes in the variance of residuals as they were reflected as changes in the slope of the cumulative variance line. The soil moisture range with flatter slopes indicated lower variability or coupled range, and vice versa.

To get an impression of the similarity in soil moisture at 5 cm and 20 cm during coupled and decoupled conditions, the ratio between two was computed as a simple quantitative measure of correspondence. A Bayesian approach, developed and explained in detail by Kruschke (2013), was applied to determine the probabilistic mean of these ratios. The mean of 5–20 cm ratio is the parameter of interest that will be estimated. Briefly, the method involved Monte Carlo Markov Chain (MCMC) to generate a large representative sample (100,000 samples) to approximate the posterior distribution of the parameter of interest. From the posterior distribution, the mean as well as the high density interval (HDI), where 95% of the estimates lie was calculated. MCMC sampling was performed separately for the coupled and decoupled range.

#### 3.2.2. Cone index seasonal variability

We also investigated if there is a trend in CI values over a growing season using the median and interquartile range (IQR) of CI over the topsoil (upper 20 cm values). This was performed for four fields where the most frequent measurements were made. These fields are RM07, RM08, TW02, and TW10. TW02 is a grass field while the other three are cultivated fields (see Table 1). We accounted for differences in soil moisture by correcting CI values to a single soil moisture value based on the method of Busscher et al. (1997). Visual assessment of the median and IQR for different dates was performed to compare CI values and to identify if there are trends over the growing seasons of 2016 and 2017.

### 3.3. Probabilistic framework to model field trafficability

A probabilistic approach was applied in identifying trafficable conditions, This allowed for the variabilities encountered in the in situ measurements to be incorporated in the analysis. First, we determined the joint empirical probability density function (pdf) for cone index and surface soil moisture using kernel density estimation (KDE). The pdf's were then utilized to calculate the conditional probabilities to express field trafficability.

#### 3.3.1. Estimating joint probability density function (pdf) for CI and surface soil moisture

We selected a subset of the in situ measurement points using the coupled range identified in Section 3.2.1. At this range, surface soil moisture can be directly related to CI as it is a good indicator of values for the whole topsoil. In situ measurement points that belong to the decoupled range were discarded.

Initial visual inspection of the measurement values revealed that those collected from grass fields tend to have higher cone index values than those in cultivated fields. The probabilistic method in Section 3.2.1 was applied and extended to test whether these measurements indeed form two separate groups, and merited separate analyses. This method is similar to a *t*-test with the main goal of determining whether the CI values are distinct from each group. The posterior distributions of grass and cultivated field were estimated using MCMC, also using 100,000 representative samples. To test the similarity between these two groups, the difference of means between every combination of representative values was obtained. Two groups were deemed similar if the difference between the means between their posterior distribution were close to or equal to zero.

kernel density estimation (KDE) was applied afterwards to determine the empirical bivariate distribution of surface soil moisture and cone index. This is a non-parametric method to estimate the underlying probability density function (pdf) of a random variable (Parzen, 1962; Rosenblatt, 1956) using kernels. It is a suitable method for datasets with complicated distribution since no assumption is made on the shape of the underlying density function. Density estimation is carried out by centering a kernel at the location of each data point. The overall density estimate is obtained by summing all the densities estimated at each point. Points that plot closer to each other will have more kernels centered nearby which yields higher density estimates.

In the bivariate case, the data points were represented by two vectors $x_1 = [x_{11}, x_{12}, x_{13}, \ldots, x_{1n}]$ and $x_1 = [x_{21}, x_{22}, x_{23}, \ldots, x_{2n}]$ where $x_i = (x_{1i}, x_{2i})$ was a sample from a bivariate distribution $f$. These two vectors represent the datasets collected for surface soil moisture and CI. The bivariate kernel density estimator $f$ was given by:

$$\hat{f}(x, \mathbf{H}) = \frac{1}{n}\sum_{i=1}^{n} K_{\mathbf{H}}(x - x_i) \tag{5}$$

where $K_H$ is a non-negative kernel function and $H$ is the kernel bandwidth that controls the amount of smoothing.

To calculate the joint pdf of soil moisture and CI using KDE, we utilized a Gaussian kernel with bandwidths (represented by $h$ for a univariate case) obtained using Scott's rule (Scott, 1992). For cultivated fields, we obtained a value of $h_{SM} = 0.022\,\mathrm{cm}^3\,\mathrm{cm}^{-3}$ and $h_{CI} = 0.138\,\mathrm{MPa}$; and for grass fields, we obtained $h_{SM} = 0.001\,\mathrm{cm}^3\,\mathrm{cm}^{-3}$ and $h_{CI} = 0.184\,\mathrm{MPa}$. From the joint pdf of CI and soil moisture, we generated 500 random samples from a multivariate normal distribution using the bandwidth matrix derived (Gentle, 2009). The random samples were drawn with replacement along the length of $x$(total number of paired data points), and then adding random noise or perturbations to the sampled values using bandwidth matrix $H$. These random samples were used to calculate the conditional probabilities.

#### 3.3.2. Determining conditional probabilities for CI to express trafficability

For a given soil moisture, we calculated the cumulative conditional probability that the corresponding CI will take a value less than or equal to a known threshold. Higher probability values indicated poor trafficability. We used a value from Droogers et al. (1996) who applied 0.70 MPa as the threshold for conditions suitable for agricultural traffic. Using the randomly generated points, trafficability is evaluated using the conditional cumulative distribution function (ccdf) given by $F_{X|A}$. This expressed the cumulative probability of a random variable $X$ conditioned on the occurrence of an event $A$:

$$F_{X|A}(x) = P(X \leq x|A) \tag{6}$$

In this case, we determined the cumulative probability that a cone index value $X$ will less than or equal to $x = 0.7\,\mathrm{MPa}$ given a soil moisture value $A$. Higher probability values indicate conditions not favorable for traffic, vice versa. Based on the results obtained in Section 4.1, soil moisture from Sentinel-1 images were transformed into its corresponding probability values for trafficability.

## 4. Results and discussion

### 4.1. Surface soil moisture from Sentinel-1

Fig. 4 shows the calculated accuracy metrics for using the four aggregation methods applied. The plot shows improvement in accuracy in all four metrics when larger pixel sizes are used compared to the

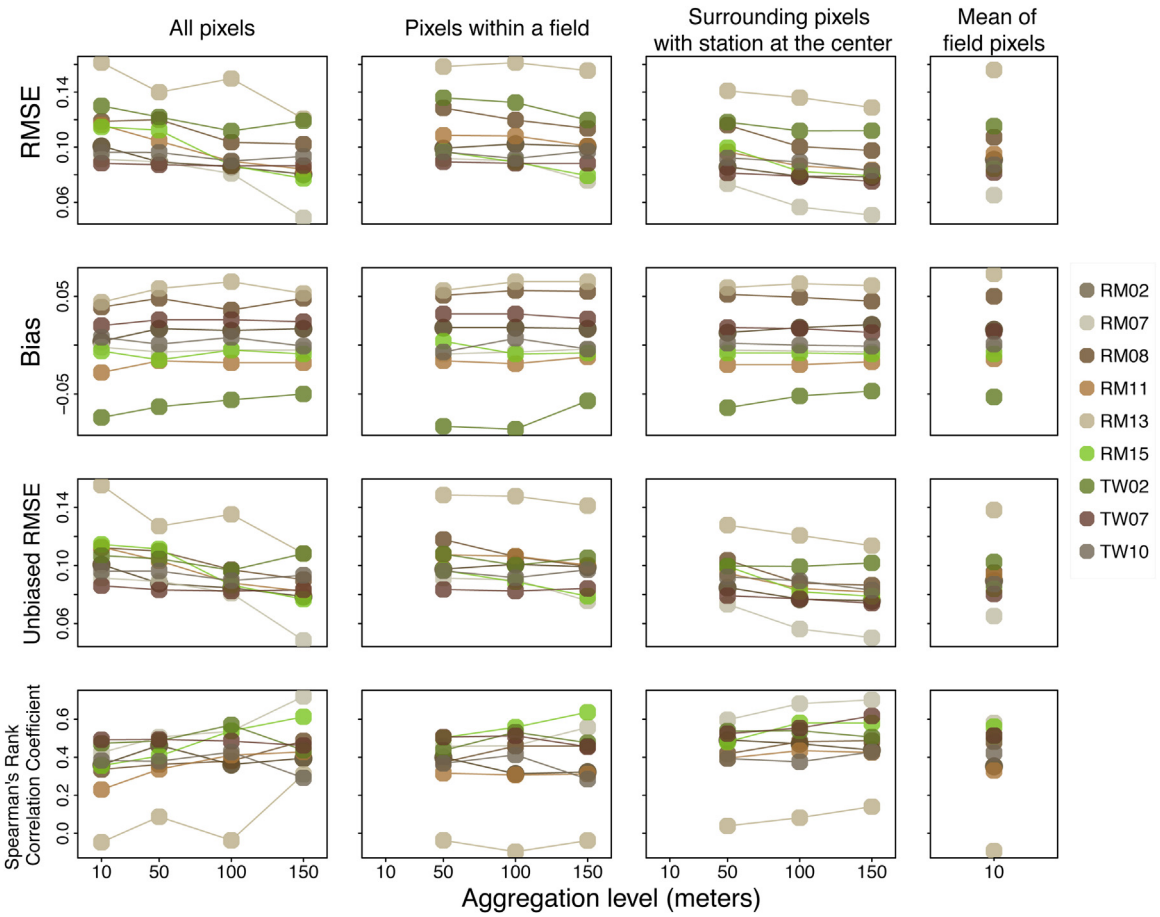


**Fig. 4.** Plots of four accuracy metrics used to compare the aggregation schemes and resolutions tested. RMSE, bias, unbiased RMSE, and Spearman's rank correlation coefficient were computed to compare the results. All metrics are in $cm^3cm^{-3}$, except for Spearman's rank correlation coefficient which is unitless. (For interpretation of the references to color in the text, the reader is referred to the web version of this article.)

original 10 m pixel size of Sentinel-1. Values for RMSE, bias, and unbiased RMSE are lower while Spearman's correlation is higher for larger pixel sizes compared to the original 10 m Sentinel-1 pixel size. From the four resolutions tested, using 150 m pixel resolution provides the best results. Furthermore, aggregation of all the pixels in a scene results in slightly higher accuracy values for all the study sites. We observed smaller variability for each metric calculated when aggregating all the pixels in a scene compared to the other methods. Radiometric uncertainties at the field scale, which affect the soil moisture retrieval accuracy, may be influenced by speckle effects (Ulaby et al., 1986). Aggregation of the original Sentinel-1 observations to larger pixels sizes implies a larger number of independent samples that leads to the suppression of speckle effects; this is critical for improving $\sigma^o$ uncertainties. Our results are in line with other studies who showed that aggregation of SAR pixels produced better results. For instance, Pierdicca et al. (2013) obtained higher soil moisture retrieval accuracy when aggregating pixels to field scale using synthetically generated $\sigma^o$ representing Sentinel-1 observations of bare soil. Pathe et al. (2009) found that retrieval errors may be dominated by noise in SAR measurements, even when assuming high model parameter errors to account for the neglect of vegetation effects. They further suggested that several pixels should be averaged to decrease the noise level, even at the expense of the spatial resolution of the soil moisture maps.

For the different land cover types, we see no apparent trend in the results. For instance, points in Fig. 4 for grass (green points) and cultivated fields (brown points) do not reveal any clustering from the plots; which implies that the accuracy of soil moisture retrievals from Sentinel-1 is comparable for grass and cultivated fields.

Aside from soil moisture, a component of the total radar backscatter is due to the influence of surface roughness and vegetation. In cultivated fields, tillage activities at the beginning of a growing season effect changes to surface roughness. Based on field measurements, Callens et al. (2006) showed that after the onset of the first rainfall events, surface roughness remains fairly stable. A sensitivity analysis performed by Joseph et al. (2010) on soil moisture retrieval across the corn growth cycle also came to a similar conclusion. In grass fields and meadows, surface roughness may be considered invariable over longer periods of time; an assumption frequently adopted in soil moisture retrieval methods (e.g. Álvarez-Mozos et al., 2006; van der Velde et al., 2012). The magnitude of vegetation effects on the total backscatter depends on sensor specifications (e.g. frequency, incidence angle, polarization) and vegetation type. Effects of grass on $\sigma^o$ is generally expected to be weak because the dimensions of scatterers (i.e. leaves and stems) are small in comparison to the SAR wavelength (e.g. Van der Velde and Su, 2009). However, the effects may be significant in cultivated fields. For example, Joseph et al. (2010) quantified the effect of corn across its growth cycle on C- and L-band backscattering at incidence angles of 15°, 35° and 55°. They showed that throughout the corn growth cycle, both an attenuated soil return and vegetation scattering can dominate the measured $\sigma^o$. However, the measured $\sigma^o$ still displayed some sensitivity to soil moisture even at peak biomass. Despite the known impacts of surface roughness and vegetation, previous studies have shown that change detection method can reasonably track changes in soil moisture using multi-temporal satellite imagery (e.g. Moran et al., 2000; Baghdadi et al., 2007; Pathe et al., 2009) since it tries to overcome the difficulties in applying bare soil and vegetation backscatter

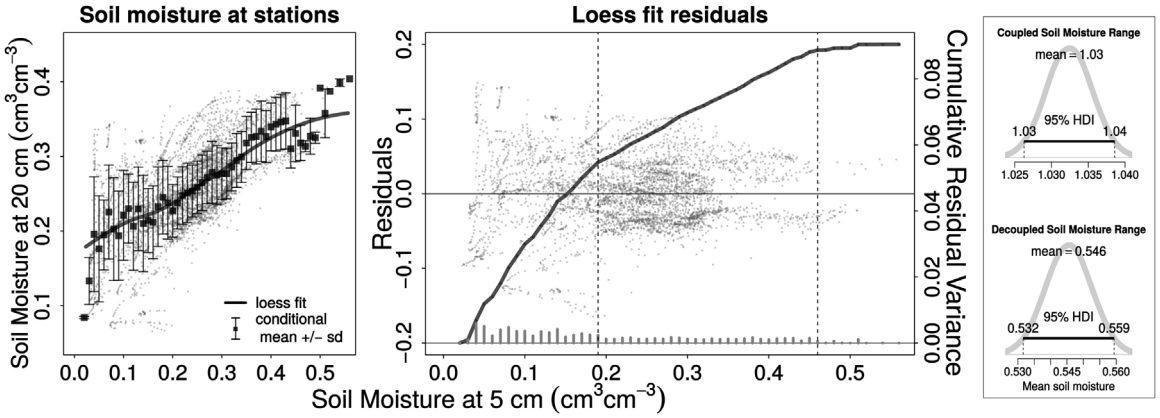


**Fig. 5.** *Left*: Scatterplot of 5 cm and 20 cm soil moisture values. 5 cm values represent surface soil moisture while 20 cm values represent the topsoil. A loess function is fitted for the overall trend while standard deviation bars indicate the variability across the whole soil moisture range. *Center*: Plot of the residuals from the fitted loess function over the surface soil moisture range. The variance from the residuals for every 0.01 $cm^3\ cm^{-3}$ interval is given by the vertical bars at the bottom of the plot. The cumulative variance of residuals is plotted as a black line. A change in the slope of the line at 0.19 $cm^3\ cm^{-3}$ separates the decoupled range ($< 0.19\ cm^3\ cm^{-3}$) from the coupled range ($\geq 0.19\ cm^3\ cm^{-3}$). *Right*: Posterior distributions of 5 to 20 cm soil moisture ratio has a mean of 1.03 $cm^3\ cm^{-3}$ for coupled range compared to 0.55 $cm^3\ cm^{-3}$ for decoupled range. The distributions also show the range corresponding to the 95% high density interval of the ratios calculated.

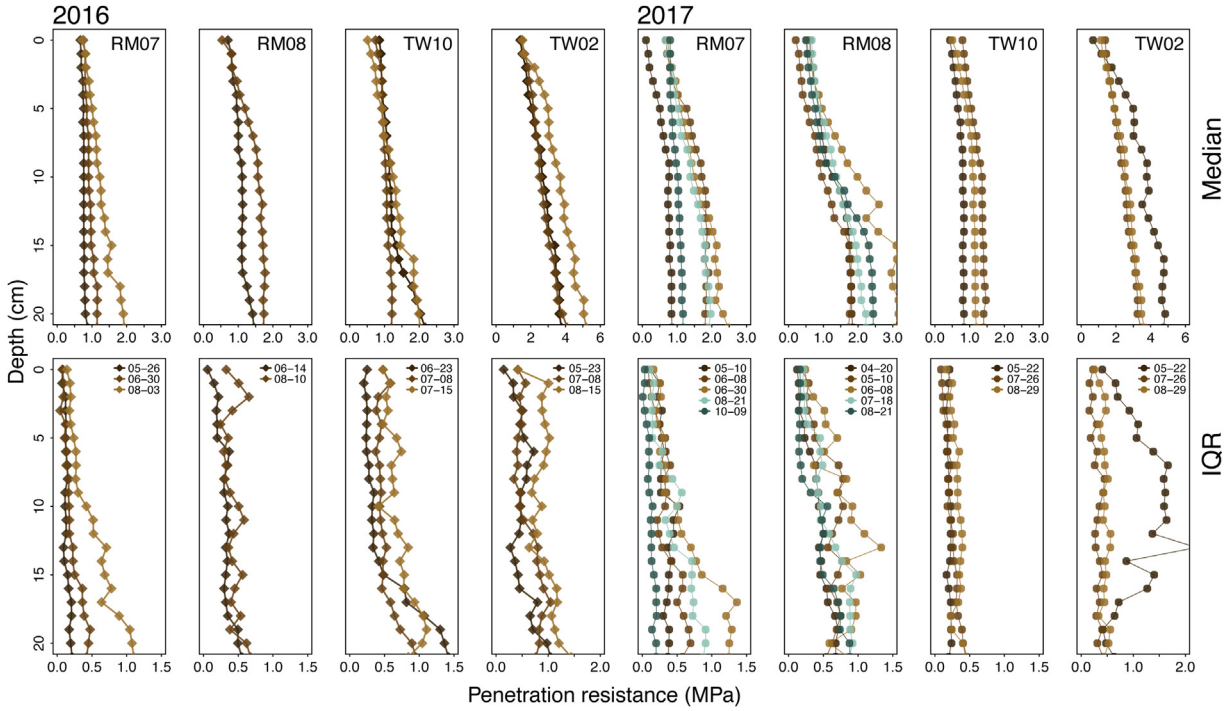


**Fig. 6.** Profile CI values at four selected fields where most measurements were collected. The top panel shows the median CI per depth per measurement date (mm–dd) while the bottom panel shows the interquartile range (IQR). Dates when the measurements are collected are indicated in the bottom panel. For 2016 and 2017, a slight increase in both median and IQR of CI is observed up to mid-growing season (brown colors). These values decrease towards the end or after harvesting (blue colors). This pattern is observed for the three sites which are cultivated fields, with exception of TW02 which is a grass field. (For interpretation of the references to color in this figure legend, the reader is referred to the web version of this article.)

models by only interpreting changes in backscatter rather than absolute backscatter levels.

For the performance of linear transformation applied (see Eq. (4)), the accuracy might vary depending on the actual soil moisture distribution. At the study sites, the range of soil moisture encountered span from dry to wet conditions, which are close to the $\theta_{wp}$ and $\theta_{sat}$ parameter values applied. However, in regions where soil moisture distribution is skewed (e.g. very dry or very wet climates), the linear transformation method might not be the optimal choice if the range of soil moisture values encountered is limited, and $\sigma_{Min}$ and $\sigma_{Max}$ are not measured under conditions of $\theta_{wp}$ and $\theta_{sat}$. In such cases, another transformation may be more appropriate. For instance, cumulative distribution function (cdf) matching (Reichle and Koster, 2004) can be applied as this method allows to incorporate the soil moisture distribution in scaling $S_w$ values.

### 4.2. Soil moisture and cone index variability

The scatterplot in Fig. 5(left) shows a general linear trend across the soil moisture range. The variability across the soil moisture range is not constant based on the length of the standard deviation bars. However, it is not very easy to visualize trends in variability from the scatterplot

alone. Further examination of the variance of residuals from the fitted loess function (Fig. 5, center) reveals that for dry conditions, variance is consistently higher compared to those during wet conditions. A change from higher to lower variance occurs at 0.19 $cm^3\,cm^{-3}$ based on the change in slope in the cumulative variance line. From this, we determine that values from $< 0.19\,cm^3\,cm^{-3}$ corresponds to a decoupled soil moisture range while those $\geq 0.19\,cm^3\,cm^{-3}$ corresponds to the coupled range (Carranza et al., 2018).

For assessment of trafficability, wetter soil moisture conditions are of primary interest since soils are generally more susceptible to compaction. During wet conditions, we found coupling between surface and topsoil soil moisture values, therefore the former is a good representative of the total soil moisture within the latter. This is further confirmed by the probabilistic mean calculated. A value equal to 1.036 $cm^3\,cm^{-3}$ for the 5–20 cm ratio (Fig. 5, right) indicates an almost 1:1 correspondence between the two. This implies that surface soil moisture, for instance those derived from Sentinel-1, can already be used as a proxy for topsoil values without the need for a separate analysis to convert surface values to topsoil soil moisture content. For the decoupled range, the probabilistic mean is 0.547 $cm^3\,cm^{-3}$, which means that subsurface values can be twice as much as the surface.

CI plots over the topsoil for four fields show the variability over a growing season Fig. 6. CI values in cultivated fields increase in median and IQR towards mid-growing season and then decreases at the end or after harvest. This shows that CI becomes higher and more variable mid-growing season when the crops are mature. However, this trend was not observed in the grass field (TW02). Aside from soil moisture, we hypothesize the root growth affects the temporal variability of CI for cultivated fields. For the grass field, the lack of trend observed is still inconclusive since we only had one site. Several studies have already looked at importance of roots in increasing soil strength, but has been investigated mainly in relation to erosion and hazards (De Baets et al., 2008; Fan and Su, 2008; Mickovski et al., 2009). Studies investigating the impact of root growth on soil hydraulic properties and field trafficability is still rare in literature (e.g. Wieder and Shoop, 2017).

### 4.3. Probabilistic modeling of field trafficability

The calibrated values plotted in Fig. 7(left) show that grass fields have higher CI values compared to those in cultivated fields. These two groups also show different probabilistic mean CI, which warrants separate analysis for trafficability (Fig. 7, right). Grass fields have a probabilistic mean CI of 1.74 MPa while cultivated fields have 0.709 MPa. The posterior distribution of the mean CI for cultivated and grass fields do not overlap and differ by at least 1 MPa. This difference can be attributed to the type of land management in these fields. For cultivated fields, yearly tillage loosens the soil so that CI values become lower at the beginning of the growing season. For grass fields, regular mowing and trampling of animals results in higher CI. Fields which remain as grass fields become more compacted over time as they are not being tilled. Faunal activities (e.g. from burrowing animals) may alleviate soil compaction to a certain degree but based on our measurements, these are not enough for grass fields to have similar CI values to cultivated fields.

Fig. 8 shows the bivariate pdf's obtained and random samples generated for cultivated and grass fields. Aside from having generally higher values, grass fields also have higher variability as seen from the spread of points in the scatterplot (Fig. 7) and bivariate pdf's (Fig. 8). The variability observed in the pdf's implies that CI values does not depend on soil moisture alone. Aside from soil moisture, bulk density also controls CI values but was implicitly incorporated when we separated the analysis for cultivated and grass fields. The differences in CI for cultivated and grass fields already indicate their differences in bulk densities.

The distribution of random samples closely approximate the original measurement data distribution CI but not for soil moisture (Fig. 8, bottom panel). However, the soil moisture values from the random samples generated seem to approximate the realistic range and distribution of soil moisture. This was confirmed by also plotting the 5 cm time series measurements from both Raam and Twente networks (plot not shown). In addition, our measurements might also be incomplete since we were not able to encounter all possible soil moisture values. From Fig. 7, we lack measurements beyond 0.4 $cm^3\,cm^{-3}$ for grass and between $\sim 0.35$–$0.4\,cm^3\,cm^{-3}$ for cultivated fields. Nevertheless, we were still able to generate random samples from the underlying distribution of soil moisture with the bandwidths used (see Section 3.3.1).

The pdf's generated over the study two-year period only reflect average/normal weather conditions in the Netherlands, which is characterized by having moderate rainfall over the whole year. Similar to our measurements (Fig. 8), intermediate soil moisture values (20–30 $cm^3\,cm^{-3}$) are the most frequent while very dry and very wet conditions occur less frequently. Therefore, the pdf's obtained are more

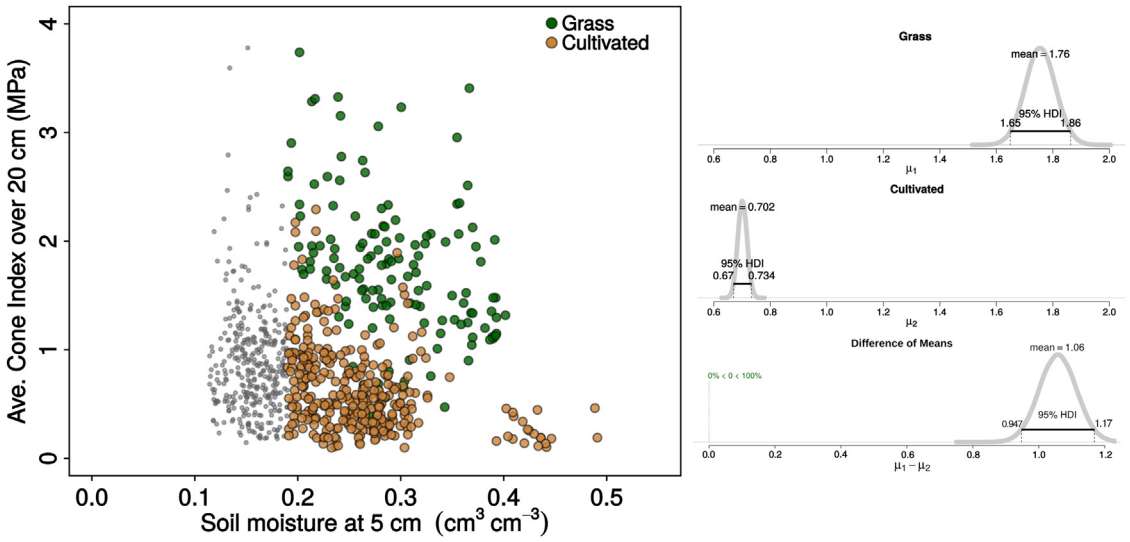


**Fig. 7.** *Left*: Scatterplot of in situ measurements of surface soil moisture and penetration resistance. Colored points are within the coupled soil moisture range while grey points are in the decoupled range. *Right*: Distribution of the probabilistic mean CI for grass and cultivated fields. The difference in mean CI for these two groups is given in the bottom panel. The probability that the difference between these two sets of mean CI is zero is also equal to zero. (For interpretation of the references to color in this figure legend, the reader is referred to the web version of this article.)

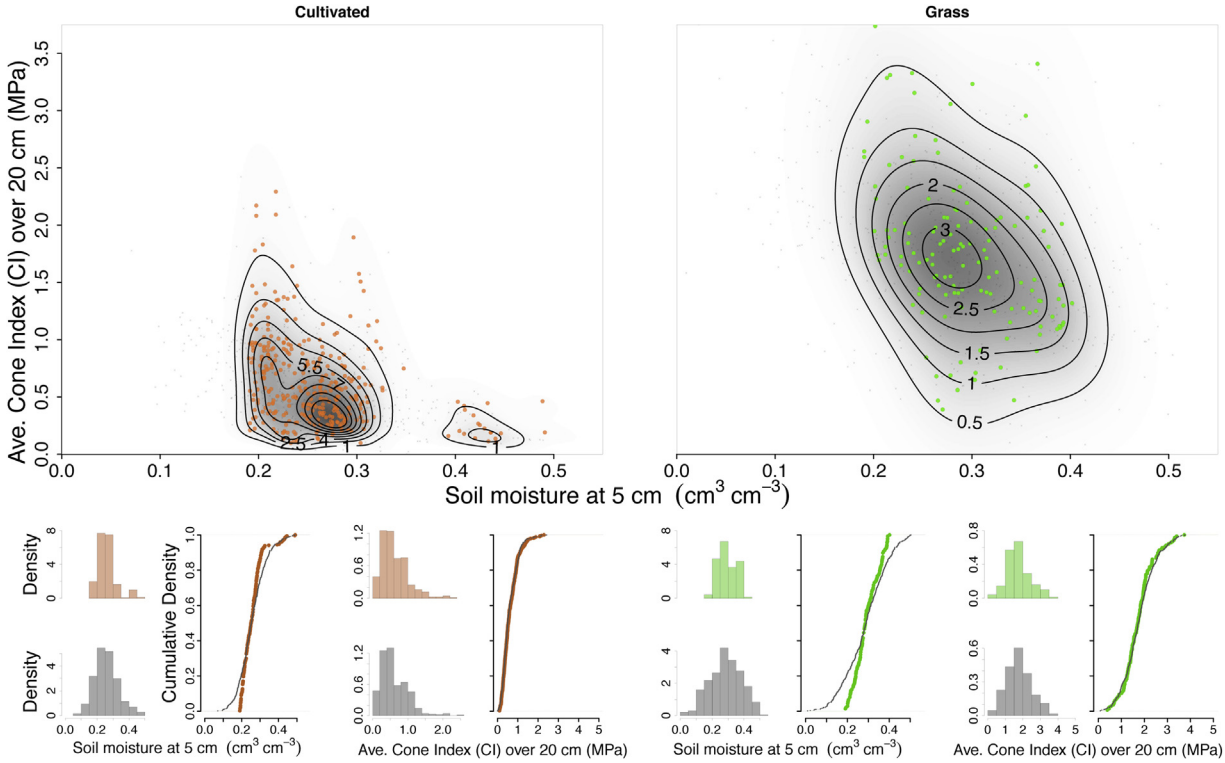


**Fig. 8.** *Top*: Plots of the joint pdf's of surface soil moisture and cone index generated by kernel density estimation for cultivated *(left)* and grass fields *(right)*. Colored points are measurement data while grey points are random samples drawn using the joint pdf's. Contour lines indicate the density of points. *Bottom*: Histograms and cumulative distribution function (cdf's) of in situ measurements and random samples drawn are plotted for comparison. (For interpretation of the references to color in this figure legend, the reader is referred to the web version of this article.)

suitable for predicting trafficability during average weather years. Since the shape of the pdf used is not universal, the results of the analysis may be suboptimal for periods when or areas where very wet or very dry weather conditions are prevalent. Modeling trafficability for such conditions can be done if the appropriate bivariate pdf's can be selected.

As for the trend in soil strength values over the whole soil moisture range, we observed that it is consistent with previous studies (Henderson et al., 1988; Vaz et al., 2011). They have shown as increasing CI trend towards drier conditions. Our findings are similar despite using only surface soil moisture values. This further strengthens the potential for using satellite-derived surface soil moisture for monitoring field trafficability.

### 4.4. Monitoring trafficability with Sentinel-1

A small area around the vicinity of RM07 in the Raam catchment is selected as a test site to demonstrate monitoring of trafficability in grass and cultivated fields Fig. 9 (top panel). Here we show the plots at four locations (2 in grass and 2 in cultivated fields). A 150 m pixel resolution was used based on the results in Section 4.1. The time series plots in Fig. 9 show soil moisture at the center of each selected field. Changes in the status of trafficability is easily observed from the high temporal resolution of Sentinel-1. Although in 2016, available Sentinel-1 imagery was lesser compared to 2017. Probability values for cultivated fields are much higher compared to grass fields even though the range of soil moisture encountered for both types of fields were the same. Soil moisture at the four selected locations all show seasonality but inter-field variability is larger for cultivated fields compared to grass fields. We also observed the same inter-field variability for other locations (both grass and cultivated fields) in this selected area (plot not included here).

From the time series plots in Fig. 9, we can identify time periods with lower probability values which translates to good trafficability conditions. For the two cultivated fields, this is observed in early spring (around April) of 2017. This also coincides with the timing of tillage for some fields in the Netherlands. For spring of 2016, however, the trafficability conditions between these two cultivated fields vary. For C1, soil moisture conditions indicate good trafficability, while for C2 it is the opposite case. The soil moisture in C2 did not decrease, so the trafficability conditions did not improve over the spring period. This difference may due to types of crops grown as well as how these fields were managed in previous years.

Grass fields always appear to be trafficable given the threshold value used. This is not the case for cultivated fields where there are more pronounced fluctuations in trafficable conditions. However, the results for grass fields may not always hold true, especially for tractors with very heavy weights. In principle, these vehicles are legally allowed to reach up to 21 tons per axle (EU Regulation 167/2013). In contrast to our results for grass fields, the soil may not be trafficable for very heavy vehicles during saturated conditions. The threshold value we used may be a more reasonable indicator of trafficability using average tractor weights ranging from 6-8 tons.

These results could potentially be used by farmers and water managers alike. For farmers, the results can be used to identify periods suitable for traffic and to aid in deciding when to initiate tillage activities. Although in practice, this might still be difficult to apply since farmers still need to work on their fields despite conditions unfavorable for traffic. Nevertheless, the results can help in increasing awareness as to when soils are more susceptible to compaction. For water managers, the results could aid in their decisions to adjust water levels in channels and/or canals in order to meet the water demands of farmers.

## 5. Conclusion

In this paper, we demonstrated how Sentinel-1 can be used to monitor trafficability status in agricultural fields. Our findings show

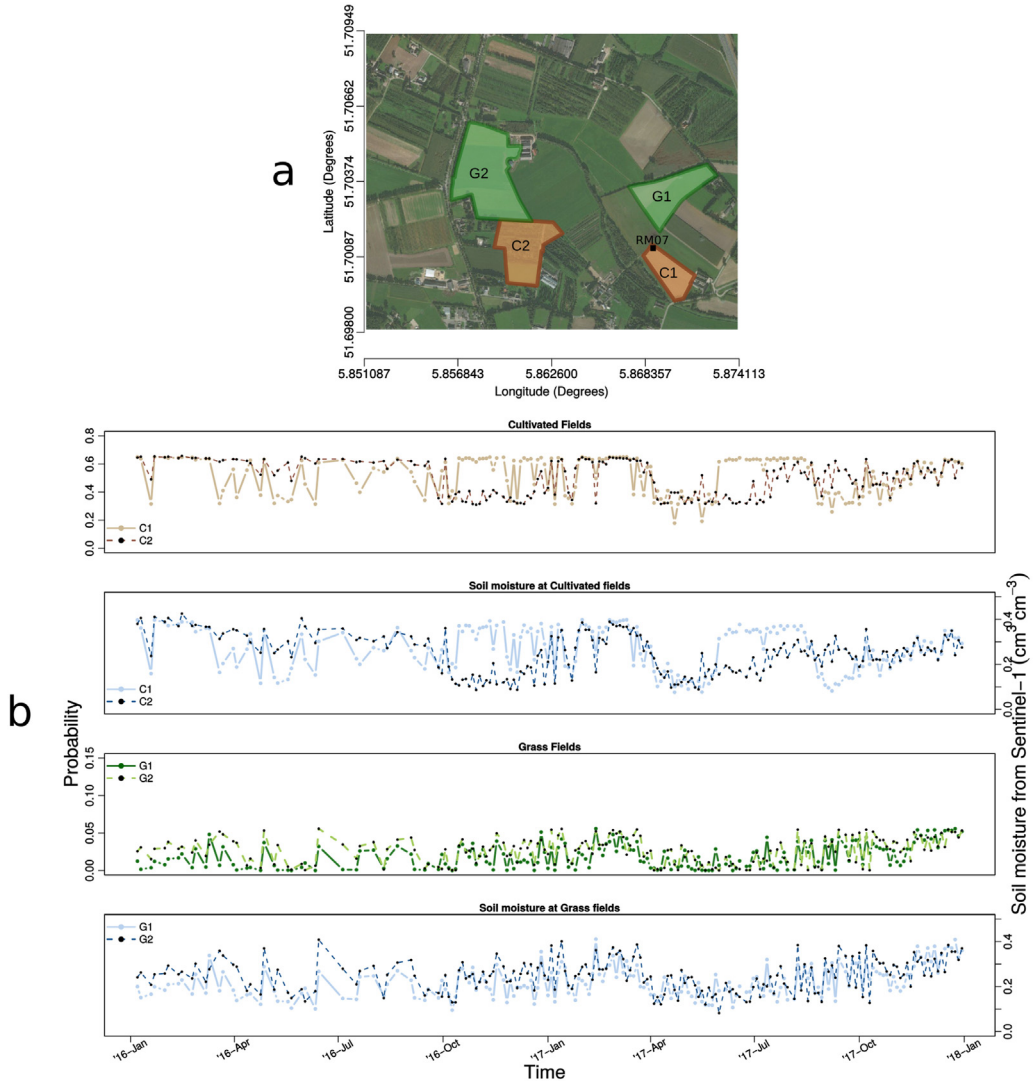


**Fig. 9.** Plot as an example for for monitoring field trafficability. (a) Map of the vicinity of RM07 station within the Raam soil moisture network where a few fields were selected. Two in grass (labeled *G*) and two in cultivated (labeled *C*) fields. One of the fields (C1) is also the location of RM07. (b) Times series plots for the probability values to express trafficability at the selected fields. Surface soil moisture derived from Sentinel-1 are also plotted (blue colors). (For interpretation of the references to color in this figure legend, the reader is referred to the web version of this article.)

that by identifying coupled conditions, satellite-derived surface soil moisture can be directly related with cone index values. Since we focused only on soil moisture as the dominant temporal control, expressing trafficability as probability values is advantageous because uncertainties are already incorporated. However, further attention should be given to the impacts of root growth as it may also act as a significant temporal control for cone index. Finally, we showed that the high temporal resolution of Sentinel-1 is suitable for tracking the changes in agricultural field trafficability. However, our results show that aggregation to coarser resolution may be necessary, which may also preclude identifying the spatial variability within a field.

## Acknowledgements

This work is part of the research programme Optimizing Water Availability through Sentinel-1 Satellites (OWAS1S) with project number 13871 which is (partly) financed by the Netherlands Organization for Scientific Research (NWO). We are grateful for the two reviewers whose comments helped improve our manuscript.

## References

Álvarez-Mozos, J., Casal í, J., González-Audícana, M., Verhoest, N.E., 2006. Assessment of the operational applicability of radarsat-1 data for surface soil moisture estimation. IEEE Trans. Geosci. Remote Sens. 44 (4), 913–924.

ASAE EP542, F., 1999. Procedures for Using and Reporting Data Obtained With the Soil Cone Penetrometer. American Society of Agricultural and Biological Engineers Tech. Rep.

Ayers, P., Perumpral, J., 1982. Moisture and density effect on cone index. Trans. ASAE 25 (5), 1169–1172.

Baghdadi, N., Aubert, M., Cerdan, O., Franchistéguy, L., Viel, C., Eric, M., Zribi, M., Desprats, J., 2007. Operational mapping of soil moisture using synthetic aperture radar data: application to the touch basin (France). Sensors 7 (10), 2458–2483.

Baghdadi, N., El Hajj, M., Zribi, M., Bousbih, S., 2017. Calibration of the water cloud model at c-band for winter crop fields and grasslands. Remote Sens. 9 (9), 969.

Bauer-Marschallinger, B., et al., 2018. Soil moisture from fusion of scatterometer and sar: closing the scale gap with temporal filtering. Remote Sens. 10 (7). https://doi.org/10.3390/rs10071030.

Baumgartl, T., Horn, R., 1991. Effect of aggregate stability on soil compaction. Soil Tillage Res. 19 (2–3), 203–213.

Bengough, A.G., Campbell, D.J., O'Sullivan, M.F., 2000. Penetrometer techniques in relation to soil compaction and root growth. In: Smith, K.A., Mullins, C.E. (Eds.), Soil and Environmental Analysis: Physical Methods, Revised, and Expanded. CRC Press, pp. 377–404.

Benninga, H.-J.F., Carranza, C.D., Pezij, M., van Santen, P., van der Ploeg, M.J., Augustijn, D.C., van der Velde, R., 2018. The raam regional soil moisture monitoring network in the Netherlands. Earth Syst. Sci. Data 10 (1), 61.

Bousbih, S., Zribi, M., Lili-Chabaane, Z., Baghdadi, N., El Hajj, M., Gao, Q., Mougenot, B., 2017. Potential of sentinel-1 radar data for the assessment of soil and cereal cover parameters. Sensors 17 (11), 2617.

Busscher, W., Bauer, P., Camp, C., Sojka, R., 1997. Correction of cone index for soil water content differences in a coastal plain soil. Soil Tillage Res. 43 (3), 205–217. https://doi.org/10.1016/S0167-1987(97)00015-9.

Callens, M., Verhoest, N.E., Davidson, M.W., 2006. Parameterization of tillage-induced single-scale soil roughness from 4-m profiles. IEEE Trans. Geosci. Remote Sens. 44 (4), 878–888.

Campbell, D., O'Sullivan, M., 1991. The cone penetrometer in relation to trafficability, compaction and tillage. In: S.K.A, M.C.E (Eds.), Soil Analysis: Physical Methods. Marcel Dekker Inc., New York, pp. 399–429.

Capehart, W.J., Carlson, T.N., 1997. Decoupling of surface and near-surface soil water content: a remote sensing perspective. Water Resour. Res. 33 (6), 1383–1395.

Carranza, C.D., van der Ploeg, M.J., Torfs, P.J., 2018. Using lagged dependence to identify (de)coupled surface and subsurface soil moisture values. Water Resour. Res. 22 (4), 2255–2267. https://doi.org/10.5194/hess-22-2255-2018.

Carrara, M., Castrignanò, A., Comparetti, A., Febo, P., Orlando, S., 2007. Mapping of penetrometer resistance in relation to tractor traffic using multivariate geostatistics. Geoderma 142 (3–4), 294–307.

Cihlar, J., Ulaby, F.T., 1974. Dielectric Properties of Soils as a Function of Moisture Content. The University of Kansas Center for Research, Inc., Lawrence, Kansas Tech. Rep. 177-4.

De Baets, S., Poesen, J., Reubens, B., Wemans, K., De Baerdemaeker, J., Muys, B., 2008. Root tensile strength and root distribution of typical mediterranean plant species and their contribution to soil shear strength. Plant Soil 305 (1–2), 207–226.

Dente, L., Vekerdy, Z., Su, Z., Ucer, M., 2011. Twente Soil Moisture and Soil Temperature Monitoring Network. University of Twente, Netherlands.

Droogers, P., Fermont, A., Bouma, J., 1996. Effects of ecological soil management on workability and trafficability of a loamy soil in the netherlands. Geoderma 73 (3–4), 131–145.

Earl, R., 1997. Prediction of trafficability and workability from soil moisture deficit. Soil Tillage Res. 40 (3–4), 155–168.

Eckelmann, W., et al., 2006. Common Criteria for Risk Area Identification According to Soil Threats. Office for Official Publications of the European Communities.

Ekwue, E., Harrilal, A., 2010. Effect of soil type, peat, slope, compaction effort and their interactions on infiltration, runoff and raindrop erosion of some trinidadian soils. Biosyst. Eng. 105 (1), 112–118.

ESA, 2019. Copernicus Open Access Hub.

Fan, C.-C., Su, C.-F., 2008. Role of roots in the shear strength of root-reinforced soils with high moisture content. Ecol. Eng. 33 (2), 157–166.

FAO, I., 2015. Status of the World's Soil Resources (swsr)-Main Report. Food and Agriculture Organization of the United Nations and Intergovernmental Technical Panel on Soils, Rome, Italy, pp. 650.

Ferrero, A., Usowicz, B., Lipiec, J., 2005. Effects of tractor traffic on spatial variability of soil strength and water content in grass covered and cultivated sloping vineyard. Soil Tillage Res. 84 (2), 127–138.

Gentle, J.E., 2009. Computational Statistics, Chap. Generation of Random Numbers. Springer New York, New York, NY, pp. 305–331. https://doi.org/10.1007/978-0-387-98144-4.

Hajj, M.E., Baghdadi, N., Zribi, M., Bazzi, H., 2017. Synergic use of sentinel-1 and sentinel-2 images for operational soil moisture mapping at high spatial resolution over agricultural areas. Remote Sens. 9 (12), 1292.

Hamza, M., Anderson, W., 2005. Soil compaction in cropping systems: a review of the nature, causes and possible solutions. Soil Tillage Res. 82 (2), 121–145.

Henderson, C., Levett, A., Lisle, D., 1988. The effects of soil water content and bulk density on the compactibility and soil penetration resistance of some western Australian sandy soils. Soil Res. 26 (2), 391–400.

Hornacek, M., Wagner, W., Sabel, D., Truong, H.-L., Snoeij, P., Hahmann, T., Diedrich, E., Doubková, M., 2012. Potential for high resolution systematic global surface soil moisture retrieval via change detection using sentinel-1. IEEE J. Sel. Top. Appl. Earth Obs. Remote Sens. 5 (4), 1303–1311.

Hupet, F., Vanclooster, M., 2002. Intraseasonal dynamics of soil moisture variability within a small agricultural maize cropped field. J. Hydrol. 261 (1–4), 86–101.

Joseph, A., van der Velde, R., O'neill, P., Lang, R., Gish, T., 2010. Effects of corn on c-and l-band radar backscatter: a correction method for soil moisture retrieval. Remote Sens. Environ. 114 (11), 2417–2430.

Keller, T., Lamandé, M., 2010. Challenges in the development of analytical soil compaction models. Soil Tillage Res. 111 (1), 54–64.

Knight, S., Freitag, D., 1961. Measuring Soil Trafficability Characteristics. Army Engineer Waterways Experiment Station Vicksburg MS Tech. Rep.

Kornelsen, K.C., Coulibaly, P., 2013. Advances in soil moisture retrieval from synthetic aperture radar and hydrological applications. J. Hydrol. 476, 460–489.

Kruschke, J.K., 2013. Bayesian estimation supersedes the t test. J. Exp. Psychol. Gen. 142 (2), 573.

Kuang, B., Mahmood, H.S., Quraishi, M.Z., Hoogmoed, W.B., Mouazen, A.M., van Henten, E.J., 2012. Chapter four – sensing soil properties in the laboratory, in situ, and online: a review. In: In: Sparks, D.L. (Ed.), Advances in Agronomy, Advances in Agronomy, vol. 114. Academic Press, pp. 155–223.

Lal, R., 1991. Tillage and agricultural sustainability. Soil Tillage Res. 20 (2–4), 133–146.

Lievens, H., Verhoest, N.E., Keyser, E.D., Vernieuwe, H., Matgen, P., Álvarez-Mozos, J., Baets, B.D., 2011. Effective roughness modelling as a tool for soil moisture retrieval from c-and l-band sar. Hydrol. Earth Syst. Sci. 15 (1), 151–162.

Mickovski, S.B., Hallett, P.D., Bransby, M.F., Davies, M.C., Sonnenberg, R., Bengough, A.G., 2009. Mechanical reinforcement of soil by willow roots: impacts of root properties and root failure mechanism. Soil Sci. Soc. Am. J. 73 (4), 1276–1285.

Mladenova, I.E., Jackson, T.J., Bindlish, R., Hensley, S., 2013. Incidence angle normalization of radar backscatter data. IEEE Trans. Geosci. Remote Sens. 51 (3), 1791–1804.

Moran, M.S., Hymer, D.C., Qi, J., Sano, E.E., 2000. Soil moisture evaluation using multitemporal synthetic aperture radar (sar) in semiarid rangeland. Agric. Forest Meteorol. 105 (1–3), 69–80.

Müller, L., Lipiec, J., Kornecki, T.S., Gebhardt, S., 2011. Trafficability and workability of soils. In: Gliński, J., Horabik, J., Lipiec, J. (Eds.), Encyclopedia of Agrophysics. Springer Netherlands, pp. 912–924. https://doi.org/10.1007/978-90-481-3585-1.

Nawaz, M.F., Bourrie, G., Trolard, F., 2013. Soil compaction impact and modelling. A review. Agron. Sustain. Dev. 33 (2), 291–309.

Parzen, E., 1962. On estimation of a probability density function and mode. Ann. Math. Stat. 33 (3), 1065–1076.

Pathe, C., Wagner, W., Sabel, D., Doubkova, M., Basara, J.B., 2009. Using envisat asar global mode data for surface soil moisture retrieval over oklahoma, usa. IEEE Trans. Geosci. Remote Sens. 47 (2), 468–480.

Paul, C., de Vries, J., 1979. Prediction of soil strength from hydrologic and mechanical properties. Can. J. Soil Sci. 59 (3), 301–311.

Pierdicca, N., Pulvirenti, L., Pace, G., 2013. A prototype software package to retrieve soil moisture from sentinel-1 data by using a bayesian multitemporal algorithm. IEEE J. Sel. Top. Appl. Earth Obs. Remote Sens. 7 (1), 153–166.

Priddy, J.D., Willoughby, W.E., 2006. Clarification of vehicle cone index with reference to mean maximum pressure. J. Terramech. 43 (2), 85–96.

Raghavan, G., Alvo, P., McKyes, E., 1990. Soil compaction in agriculture: a view toward managing the problem. In: Lal, R., Stewart, B. (Eds.), Advances in Soil Science: Soil Degradation. Springer New York, New York, NY, pp. 1–36. https://doi.org/10.1007/978-1-4612-3322-0.

Rawls, W., Gish, T., Brakensiek, D., 1991. Estimating soil water retention from soil physical properties and characteristics. Advances in Soil Science. Springer, pp. 213–234.

Reichle, R.H., Koster, R.D., 2004. Bias reduction in short records of satellite soil moisture. Geophys. Res. Lett. 31 (19).

Reintam, E., Vennik, K., Kukk, L., Kade, S., Krebstein, K., Are, M., Astover, A., 2016. Measuring and predicting soil moisture conditions for trafficability. Acta Agric. Scand. 66 (8), 698–705.

Rosenblatt, M., 1956. Remarks on some nonparametric estimates of a density function. Ann. Math. Stat. 832–837.

Rücknagel, J., Hofmann, B., Deumelandt, P., Reinicke, F., Bauhardt, J., Hülsbergen, K.-J., Christen, O., 2015. Indicator based assessment of the soil compaction risk at arable sites using the model repro. Ecol. Indic. 52, 341–352.

Scott, D., 1992. Multivariate Density Estimation: Theory, Practice, and Visualization. A Wiley-Interscience Publication, Wiley.

Seneviratne, S.I., Corti, T., Davin, E.L., Hirschi, M., Jaeger, E.B., Lehner, I., Orlowsky, B., Teuling, A.J., 2010. Investigating soil moisture-climate interactions in a changing climate: a review. Earth-Sci. Rev. 99 (3–4), 125–161.

Sojka, R., Busscher, W., Lehrsch, G., 2001. In situ strength, bulk density, and water content relationships of a durinodic xeric haplocalcid soil. Soil Sci. 166 (8), 520–529.

Torres, R., et al., 2012. Gmes sentinel-1 mission. Remote Sens. Environ. 120, 9–24.

Ulaby, F.T., Moore, R.K., Fung, A.K., 1986. Microwave Remote Sensing Active and Passive-Volume II: Radar Remote Sensing and Surface Scattering and Emission Theory. Addison-Wesley Publishing Company Advanced Book Program/World Science Division.

Upadhyaya, S., 2005. Stress-strain and soil strength. In: Hillel, D. (Ed.), Encyclopedia of Soils in the Environment. Elsevier, Oxford, pp. 38–54. https://doi.org/10.1016/B0-12-348530-4/00507-5.

van der Velde, R., Salama, M.S., Eweys, O.A., Wen, J., Wang, Q., 2015. Soil moisture mapping using combined active/passive microwave observations over the east of the netherlands. IEEE J. Sel. Top. Appl. Earth Obs. Remote Sens. 8 (9), 4355–4372.

Van der Velde, R., Su, Z., 2009. Dynamics in land-surface conditions on the tibetan plateau observed by advanced synthetic aperture radar (asar). Hydrol. Sci. J. 54 (6), 1079–1093.

van der Velde, R., Su, Z., van Oevelen, P., Wen, J., Ma, Y., Salama, M.S., 2012. Soil moisture mapping over the central part of the Tibetan plateau using a series of ASAR WS images. Remote Sens. Environ. 120, 175–187.

Van Dijck, S., Van Asch, T.W., 2002. Compaction of loamy soils due to tractor traffic in vineyards and orchards and its effect on infiltration in southern France. Soil Tillage Res. 63 (3), 141–153.

van Genuchten, M.T., 1980. A closed-form equation for predicting the hydraulic conductivity of unsaturated soils 1. Soil Sci. Soc. Am. J. 44 (5), 892–898.

Vaz, C.M., Bassoi, L.H., Hopmans, J.W., 2001. Contribution of water content and bulk density to field soil penetration resistance as measured by a combined cone penetrometer-tdr probe. Soil Tillage Res. 60 (1–2), 35–42.

Vaz, C.M., Manieri, J.M., De Maria, I.C., Tuller, M., 2011. Modeling and correction of soil penetration resistance for varying soil water content. Geoderma 166 (1), 92–101.

Vereecken, H., et al., 2014. On the spatio-temporal dynamics of soil moisture at the field scale. J. Hydrol. 516, 76–96.

Wagner, W., Lemoine, G., Rott, H., 1999. A method for estimating soil moisture from ers scatterometer and soil data. Remote Sens. Environ. 70 (2), 191–207.

Wieder, W.L., Shoop, S.A., 2017. Vegetation Impact on Soil Strength: A State of the Knowledge Review. U.S. Army Engineer Research and Development Center (ERDC), Cold Regions Research and Engineering Laboratory Tech. Rep.

Wösten, J., Veerman, G., de Groot, W., Stolte, J., 2001. Waterretentie-en Doorlatendheidskarakteristieken Van Boven-en Ondergronden in Nederland: de Staringreeks; Vernieuwde Uitgave 2001. Tech. Rep., Alterra.

Wosten, J., et al., 2013. Bofek2012, De Nieuwe Bodemfysische Schematisatie Van Nederland. Tech. Rep., Alterra.